Drink. Water Eng. Sci., 7, 41–52, 2014
www.drink-water-eng-sci.net/7/41/2014/
doi:10.5194/dwes-7-41-2014


Drinking Water
Engineering and Science
Open Access

# Immobilized photocatalyst on stainless steel woven meshes assuring efficient light distribution in a solar reactor

**A. S. El-Kalliny[1,2,3], S. F. Ahmed[1], L. C. Rietveld[2], and P. W. Appel[1]**

[1]Product and Process Engineering, ChemE, Delft University of Technology, Julianalaan 136, 2628 BL Delft, the Netherlands
[2]Sanitary Engineering, Faculty of Civil Engineering and Geosciences, Delft University of Technology, Stevinweg 1, 2628 CN Delft, the Netherlands
[3]Department of Water Pollution Research, National Research Centre, Dokki, 12622 Giza, Egypt

*Correspondence to:* A. S. El-Kalliny (kalliny78@hotmail.com)

Received: 5 November 2013 – Published in Drink. Water Eng. Sci. Discuss.: 3 February 2014
Revised: – – Accepted: 6 April 2014 – Published: 3 June 2014

**Abstract.** An immobilized $TiO_2$ photocatalyst with a high specific surface area was prepared on stainless steel woven meshes in order to be used packed in layers for water purification. Immobilization of such a complex shape needs a special coating technique. For this purpose, dip coating and electrophoretic deposition (EPD) techniques were used. The EPD technique gave the $TiO_2$ coating films a better homogeneity and adhesion, fewer cracks, and a higher $^{\bullet}OH$ formation than the dip coating technique. The woven mesh structure packed in layers guaranteed an efficient light-penetration in water treatment reactor. A simple equation model was used to describe the distribution of light through the mesh layers in the presence of absorbing medium (e.g., colored water with humic acids). Maximum three or four coated meshes were enough to harvest the solar UV light from 300 nm to 400 nm with a high penetration efficiency. The separation distance between the mesh layers played an important role in the efficiency of solar light penetration through the coated mesh layers, especially in case of colored water contaminated with high concentrations of humic acid.

## 1 Introduction

The use of photocatalytic oxidation to remove organic pollutants from drinking water has attracted considerable interests in recent years (Malato et al., 2009). In particular, the use of $TiO_2$ photocatalysts for water purification has been of great interest because $TiO_2$ is stable, harmless, inexpensive, and can potentially be activated by solar radiation (Malato et al., 2009). The application of $TiO_2$ in suspension (e.g., $TiO_2$-P25 Degussa) is effective in capturing sun light, because suspended $TiO_2$ powders have a high specific surface area in the range from 50 $m^2\,g^{-1}$ to higher than 300 $m^2\,g^{-1}$ (Balasubramanian et al., 2004a; Malato et al., 2002; Sunada et al., 2003; Gumy et al., 2006; Thiruvenkatachari et al., 2008), which in turn helps in avoiding mass transfer limitations, resulting in a high photocatalytic activity (Mehrotra et al., 2003). However, a light transport limitation appears with a high catalyst loading. Besides, it is difficult to separate the small $TiO_2$ particles from water after treatment (Thiruvenkatachari et al., 2008; McCullagh et al., 2011; Feitz et al., 2000). To overcome this, the catalyst particles can be immobilized on a surface. Yet this may lower the oxidation potential per volume of water compared to the slurry system, due to mass transfer limitation and light transport limitation caused by (i) a lower catalyst surface-to-volume ratio, (ii) the presence of substrate that absorbs light and worsens its distribution, and (iii) a lack of movement of particles (Feitz et al., 2000; Dijkstra et al., 2001).

There have been many attempts to immobilize $TiO_2$ photocatalyst over different structures of supports along with increasing the surface/volume ratio at the same time, which consequently enhances the photocatalytic oxidation

efficiency. However, the surface area can only be efficient if it allows efficient absorption of light. There are different kinds of materials that have been used as a support to fix $TiO_2$, such as glass and borosilicate glass (Fujishima et al., 2008; Yang et al., 2004; Parra et al., 2004; Zhang et al., 2012; Ziegmann et al., 2006), cellulose fibres (Goetz et al., 2009), and stainless steel (Yanagida et al., 2006; Chen and Dionysiou, 2006a, b, 2007). Among the different supports, stainless steel is an excellent substrate material for many reasons. First, it keeps its structural integrity under the high temperature required for calcination of the $TiO_2$ films whereas quartz glass, for example, softens and deforms. Second, it is not susceptible to attack during the coating process (e.g., sodium ions diffused from the soda-lime glass into the $TiO_2$ film and decreased the photocatalytic activity, Nam et al., 2004). Third, stainless steel can be used in the electrochemical process whereas quartz and ceramics cannot be used because of their dielectric properties. At last, it can be easily used in complex shapes and has excellent mechanical properties (Balasubramanian et al., 2004b). The structures of substrates so far used do not allow an even light distribution in a fixed bed reactor and therefore the photocatalytic efficiency is much lower compared to that of a slurry reactor. Therefore, the challenge of designing an efficient photocatalytic reactor is in using a suitable catalyst structure to optimize both the area covered by photocatalytic particles and the light distribution. The design criteria of such a reactor should be (i) good vertical mixing, (ii) high surface area per unit reactor volume, and (iii) no shadowing effect.

A stainless steel woven mesh catalyst substrate is applied in the field of air purification as it shows a higher mechanical strength and a lower pressure drop than typical ceramic monolith honeycomb catalysts (Ismail et al., 2007). Also, Shang et al. (2003) used a stainless steel webnet coated by $TiO_2$ for the degradation of gaseous formaldehyde in a cylindrical flowing photo-reactor. This webnet structure showed a good activity due to its large surface area, good ventilation for gases passing, and good utilization of UV light. In the water purification field, the $Ti/TiO_2$ mesh structure was prepared by an anodization method and the photocatalytic efficiency was studied by several researchers (F. B. Li et al., 2002; X. Z. Li et al., 2000, 2002; Yoon et al., 2009). However, the anodization process requires a high energy input and moreover Ti mesh is expensive, which makes this technique not feasible for large-scale applications. On the other hand, although a mixture of anatase and rutile (e.g., the $TiO_2$ crystallites of Evonik (Degussa) P25 contain a combination of anatase ($\sim 80\,\%$) and rutile, $\sim 20\,\%$) gives a high photocatalytic activity due to the intimate contact between the two phases, enhances the separation of photo-generated electrons and holes, and results in a reduced recombination (Pelaez et al., 2012), yet, it is difficult to control the anatase-to-rutile ratio in the anodization process to have the highest photocatalytic activity.

In this paper, stainless steel woven meshes were selected to be a substrate for immobilization of $TiO_2$ particles. An immobilized photocatalyst was prepared by using the sol gel dip coating technique and electrophoretic deposition (EPD) technique. These immobilization techniques are suitable for coating substrates of complex shape such as woven meshes (Chen and Dionysiou, 2006c; Yanagida et al., 2005). For example, EPD was used for immobilizing $TiO_2$ over different types of substrates such as carbon and SiC fiber (Boccaccini et al., 2004), metal fiber or plate (Boccaccini et al., 2001; Sakamoto et al., 1998), and stainless steel meshes (Yanagida et al., 2005; Ghorbani, 2008). However, using stainless steel meshes coated with $TiO_2$ packed in layers in the water purification field has not been done so far. The production of $^{\bullet}OH$ radicals was detected by a photoluminescence (PL) technique in order to evaluate the performance of the coated meshes. Based on the design criteria of packed bed solar reactor, solar light transmission through the woven mesh layers in the presence of light absorbing medium such as humic acid (HA) was studied in order to determine the optimum number of mesh layers and the separation distance between them.

## 2 Experimental methods

### 2.1 Experimental approach

Immobilization of the $TiO_2$ photocatalyst over stainless steel woven meshes was done by using sol gel dip coating and EPD techniques in order to reach the best coating films with such a complex shape of the substrate. PL technique was used in order to evaluate the photocatalytic activity of the $TiO_2$ films. Besides, the thickness, the roughness, and the microscopic images of $TiO_2$ films were investigated to optimize the best coating films. Then the distribution of the solar light through the catalyst meshes structure in the presence of light non-absorbing or light absorbing medium was detected in order to optimize the number of mesh layers and the separation distance between them. The transmitted light through the mesh layers was measured and compared with the calculated values via a developed equation model to investigate its validity. The developed equation model was used for the determination of the fraction of the captured light by meshes, available for the production of $^{\bullet}OH$ radicals on the catalyst surface, with different values of dimensionless parameter representative for the separation distance between meshes and the extinction coefficient and concentration of the medium.

### 2.2 Preparation of the immobilized $TiO_2$ catalyst

#### 2.2.1 Treatment of the substrate

Uncoated 304 stainless steel meshes (wire diameter 0.355 mm, aperture diameter 0.915 mm, and open area 52 %) and flat plates (thickness 2 mm), used as substrates, were firstly rinsed with deionized water. After the stainless steel

was dried in air, ethanol (96 %, VWR International) and methyl ethyl ketone (99.8 %, Fisher Scientific) were used for further cleaning of the substrates. The clean substrates were dried at 125 °C for 24 h (Chen and Dionysiou, 2006c). The flat plate substrates were used only for characterization of $TiO_2$ films.

### 2.2.2 Sol gel dip coating method

The $TiO_2$ was immobilized onto discs of stainless steel meshes and flat plates of 5.7 cm diameter by the dip coating technique horizontally for 1 min. Besides, discs of stainless steel meshes of 16.5 cm diameter were used in light distribution experiments. The commercial sols O500 and O510 (TIPI Technology) were used for coating. Besides, a modified commercial sol was used by adding 10 g $TiO_2$ P-25 Degussa powder per 1 L of sol O500 or O510.

### 2.2.3 Electrophoretic deposition method

The $TiO_2$ was immobilized onto the stainless steel substrate meshes or flat plate discs of 5.5 cm diameter by the EPD technique using the vertical coating setup (Fig. 1a). In order to test the up-scalability, the horizontal coating setup (Fig. 1b) was used for coating of large-scale substrates of dimensions 32 cm × 19 cm. The orientation of the electrodes whether vertically or horizontally did not affect the coating process, where the mesh with the large size requires the horizontal setup to be handled more easily. The commercial sol O500 (TIPI Technology) modified with suspension AERODISP W740X (40 % P-25, Evonik Industries AG) was mixed by 5 % $v/v$ ratio and used as electrolyte. Figure 1 shows a schematic view of the EPD cells. The EPD process is a combination of two steps: (1) the motion of charged particles in a stable suspension under sufficient electric field (electrophoresis) and (2) the coagulation and deposition of the particles on the electrode (Ghorbani, 2008; Sarkar and Nicholson, 1996). The suspension of $TiO_2$ was mixed with O500 sol gel and formed a stable $TiO_2$ suspension sol gel. $TiO_2$ particles are negatively charged in the presence of the anionic surfactant which is used to stabilize the $TiO_2$ suspension. $TiO_2$ particles moved towards the anode by the action of the DC current (6 V, 2.5 A) during 1 min deposition time and then neutralized as they touch the depositing electrode or deposit and became static (Sarkar and Nicholson, 1996; Grillon et al., 1992).

### 2.2.4 Treatment of the coating films

The coating films were dried in order to adhere to the surface of the stainless steel substrate. The drying was done in a furnace by increasing the temperature at a ramp rate of 15 °C min$^{-1}$ up to 100 °C; this temperature was held for 15 min. The temperature of the furnace was subsequently increased at a ramp rate of 15 °C min$^{-1}$ to the final calcination temperature (200–600 °C) and was held at this value for 15 min. The optimum final drying temperature and the number of performed dip coatings were determined as they affect strongly the adhesion of the catalyst film over the stainless steel substrate and consequently the photocatalytic efficiency (Chen and Dionysiou, 2006c). The optimum drying temperature determined when using the dip coating technique was also used in the EPD technique. Finally, the films were cooled at ambient conditions and then rinsed by deionized water to remove any non-attached particles.

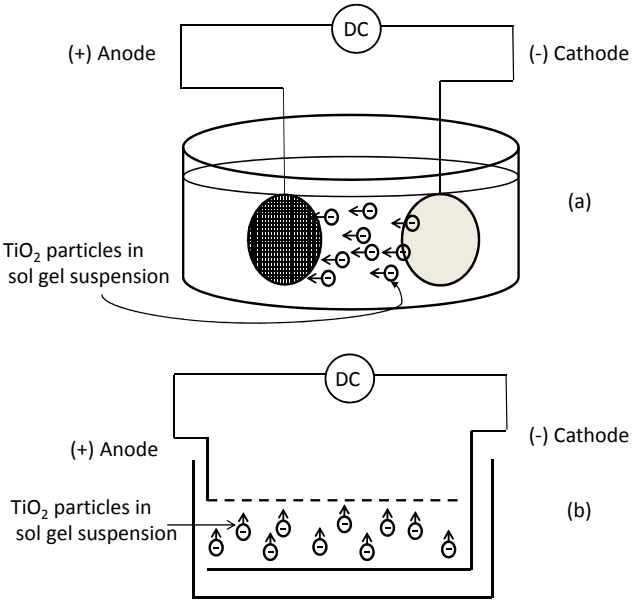


**Figure 1.** A schematic view of EPD cells. **(a)** A vertical coating setup for the small mesh discs. **(b)** A horizontal coating setup for the large-scale meshes.

## 2.3 Characterization of the $TiO_2$ coatings

Surface thickness and roughness of the $TiO_2$ film were measured with the Veeco Dektak 8 Stylus Profiler fitted with a 12.5 µm tip. Reflection of the immobilized $TiO_2$ film was detected by using the integrated sphere of UV/VIS/NIR spectrophotometer, model Lambda 90, Perkin Elmer (300–400 nm). The homogeneity of the coating layer was investigated by the optical stereo microscope "Stereo-Discovery V8" from Carl Zeiss. The adhesion of the $TiO_2$ film was investigated by using a tape casting method similar to the ASTM (ASTM D3359) test. The cross-hatch in the coating $TiO_2$ film was cut with a razor blade (single-edge #9, VWR Scientific, Media, PA, USA), followed by applying the tape (3M Scotch Tape #810) to the cross-hatch area and pulling the tape back off.

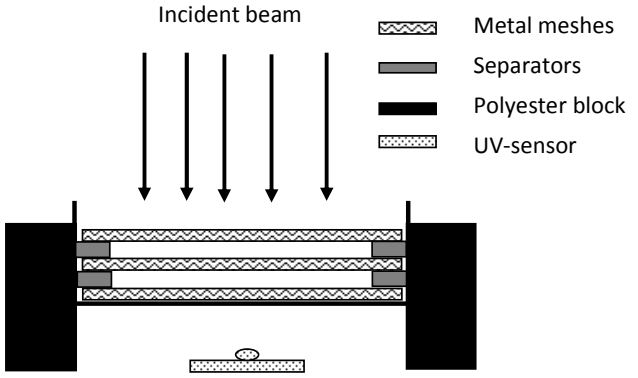


**Figure 2.** A schematic view of the experimental setup for light distribution measurements.

### 2.4 Measurements of transmitted light through the mesh structure

The apparatus designed to measure the light distribution in one or more stainless steel metal meshes with immobilized catalysts is shown in Fig. 2. The intensity of the transmitted UV solar light (300–400 nm) passing through the metal mesh, immersed in deionized water was measured by a XenoCal UV-sensor (Atlas) with a resolution of 0.1 $Wm^{-2}$. The uncoated or coated discs of metal meshes (diameter 16.5 cm) were placed in a Pyrex glass jar with an internal diameter of 18.5 cm and separated with silicone rubber rings with a height of 0.5 cm. The XenoCal UV-sensor was placed underneath the Pyrex glass vessel that was supported by a black polyester block. The Pyrex glass jar with deionized water absorbed 23 % of the intensity of the UV light in the range between 300 nm and 400 nm. The percentage of the transmitted light through the mesh layer is the ratio of the intensity of light measured by the $UV_{300-400}$-sensor through the mesh, water, and the glass vessel ($I$) to that measured through water and the glass vessel ($I_o$).

### 2.5 Theory and model equations

To calculate the light transmission through the woven meshes and the water media considering that a system in which UV radiation with an initial intensity $I_o$ ($Wm^{-2}$) falls on stacked meshes immersed in water and it was assumed that the equal distance between the meshes is such that the light transmitted through a mesh is fully homogenized before it enters the next mesh. The meshes were considered to be infinitely thin. Further, it was assumed that back and forth reflection of the light by the meshes can be neglected. Then, the intensity of the light $I_n$ ($Wm^{-2}$) on the top of $n$ meshes ($n$ is an integer) is

$$I_n = I_o(1-r)^{n-1} \cdot e^{-\varepsilon cnd}, \quad (1)$$

where $r$ (dimensionless) is the fraction of light reduced by mesh. For uncoated meshes with an open area of 52 %, $r = 0.48$. $\varepsilon$ ($L\,mg^{-1}\,cm^{-1}$) and $c$ ($mg\,L^{-1}$) are the extinction coefficient and the concentration of the medium, respectively, and $d$ (cm) is the separation distance between the meshes.

The XenoCal UV-sensor measures the intensity of the light as an integrated value over the wavelength range of 300–400 nm. Therefore, in order to compare theoretical values with experimental values, the theoretical values must also be integrated values over the same wavelength interval. The fraction of the light absorbed at a wavelength range of 300–400 nm is given by (Goldstein et al., 2007)

$$\propto = \frac{\int_{300}^{400} I(\lambda) A \mathrm{d}\lambda}{\int_{300}^{400} (\lambda) \mathrm{d}\lambda}, \quad (2)$$

where $I(\lambda)$ is the normalized photonic flux (arbitrary units) at wavelength $\lambda$ and $A(\lambda) = 1 - T(\lambda)$ is the absorbance. In order to calculate the fraction of the absorbed light $\propto$ of HA, the emission spectrum of the light $I(\lambda)$ and the transmission spectrum of the HA $T(\lambda)$ were measured over the 300–400 nm range every 0.5 nm and 2 nm, respectively (see Fig. 3). Then the integration was done numerically by approximated intervals of 2 nm width. The values of $\propto_{300-400}$, $T_{300-400}$, and $\varepsilon_{HA,300-400\,nm}$ are equal to 0.24, 0.76, and 0.028 $L\,mg^{-1}\,cm^{-1}$, respectively. The extinction coefficient $\varepsilon_{HA,300-400\,nm}$ was used to estimate the transmission through HA layers between coated mesh layers.

The value of the captured light by meshes is inversely proportional to the path length of the light through the colored medium layers ($nd$) in cm, the extinction coefficient ($\varepsilon$) in $L\,mg^{-1}\,cm^{-1}$, and the concentration ($c$) in $mg\,L^{-1}$ of the colored medium. Thus, it is essential to optimize these three factors to get as much captured light as possible.

The fraction of the captured light for a system with $n$ meshes ($\eta_n$) immersed in a light absorbing medium was determined by

$$\eta_n = \sum_{k=1}^{n} (1-r)^{k-1} \cdot e^{-k\text{ß}} \cdot r. \quad (3)$$

### 2.6 Evaluation of photocatalytic activity

Photocatalytic activity measurements were carried out by following up the $^{\bullet}OH$ formation. Hydroxyl radicals ($^{\bullet}OH$) were detected by PL using terephthalic acid (TA) from Sigma Aldrich with 98 % purity as a probe molecule. TA readily reacts with $^{\bullet}OH$ to produce a highly fluorescent product: 2-hydroxyterephthalic acid (2-OHTA) (Yu and Wang, 2010). The PL signal intensity of 2-OHTA at 425 nm is proportional to the amount of $^{\bullet}OH$ produced in water. The photocatalytic activity experiments were done with meshes in 250 mL Pyrex glass beakers (internal diameter 7 cm) using a magnetic stirrer (IKA, RT15) with an equal stirring rate at 550 rpm (rotation per minute). The temperature was controlled to be

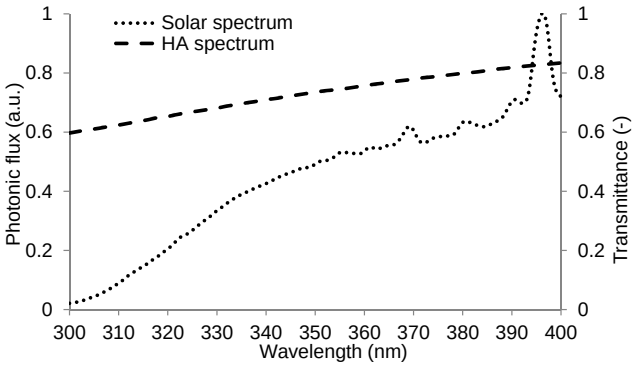


**Figure 3.** Transmission spectrum of HA was measured by Hach Lange DR 5000 spectrophotometer and the normalized emission spectrum of artificial solar light was measured by Black C-50 spectrometer, a product of StellarNet Inc.

$32 \pm 1\,^{\circ}\mathrm{C}$ by letting the water flow in a water bath through a recirculation cooler (Julabo, FL300). The entire system was placed inside the chamber of the SUNTEST XXL+ (Atlas) which consists of 3 xenon lamps irradiating UV solar light (300–400 nm) with an intensity of $40\,\mathrm{W\,m^{-2}}$. The solar spectrum of these xenon lamps was measured by a Black C-50 spectrometer, a product of StellarNet. The coated stainless steel meshes with a diameter of 5.7 cm were separated with silicone rubber rings of a diameter of 0.2 cm. The deionized water used in the preparation of TA ($5 \times 10^{-4}$ M dissolved in $2 \times 10^{-3}$ M NaOH aqueous solution) was aerated before the reaction to let the dissolved oxygen concentration reach about $8\,\mathrm{mg\,L^{-1}}$. For each experiment, 100 mL of this TA solution was stirred for 30 min with the immobilized $TiO_2$ catalyst in the dark to take the water bath temperature and to ensure equilibrium adsorption.

### 2.7 Analyses

PL spectra of generated 2-OHTA due to the reaction of TA with the $^{\bullet}$OH radicals were measured by a Photoluminescence Spectrophotometer PIT Quanta Master Model QM-1. After light irradiation for 45 min, the reaction solution was used to measure the increase of the PL intensity at 425 nm excited by 315 nm light.

The concentration of the working solution of HA in all light experiments was approximately $10\,\mathrm{mg\,L^{-1}}$. It was prepared from a $1000\,\mathrm{mg\,L^{-1}}$ stock solution of HA sodium salt (Sigma Aldrich) which was prepared by dissolving it in deionized water and filtering it through a 0.45 µm syringe-driven filter unit (Millex) to remove suspended solids ($0.03\,\mathrm{g\,L^{-1}}$). The concentration was monitored with a Hach Lange DR 5000 spectrophotometer by measuring the UV absorbance at 254 nm ($UV_{254}$), which represents the aromatic moieties (Yigit and Inan, 2009). The $UV_{254}$ calibration curve with five concentration levels of HA is shown as a straight line with $R^2$ equal to 0.991. The extinction coefficient of HA determined by Lambert Beer's law is $\varepsilon_{\mathrm{HA,254\,nm}} = 0.0717\,\mathrm{L\,mg^{-1}\,cm^{-1}}$.

## 3 Results and discussion

### 3.1 Performance and characterization of coated meshes

#### 3.1.1 Sol gel dip coating

Figure 4 shows the PL spectra of 2-OHTA formed by the reaction of TA with $^{\bullet}$OH radicals after the irradiation of the different coated meshes with UV solar light ($40\,\mathrm{W\,m^{-2}}$) for 45 min. The blank line represents the TA solution with meshes coated with O510-P25 in the dark. No PL signal was observed in the absence of UV light irradiation, which indicates that there was no formation of 2-OHTA and consequently no formation of $^{\bullet}$OH radicals. Coated films with plain sol gels O500 and O510 showed some photocatalytic activity as they contain nano $TiO_2$ particles, while those coated with sol gel modified by P25 Degussa powder gave the highest PL peak at 425 nm. The loading of P25 had considerably increased the photocatalytic activity of the plain sol gel, which is consistent with what was found by Chen and Dionysiou (2006a, b, 2007). The presence of $TiO_2$-P25 particles increased the photocatalytic activity of the coating film as P25 consists of an anatase/rutile phase mixture ratio of approximately 80/20 (Collins-Martínez et al., 2007). The mixture of these two phases is beneficial in reducing the recombination of photo-generated electrons and holes (Yu et al., 2007a, b).

Figure 5a shows the effect of the final drying temperature of one dip coated woven meshes (with O500-P25 and O510-P25 sol gels) on the maximum PL intensity at 425 nm after 45 min irradiation with solar light in the presence of basic TA solution. The drying of the coating film is necessary for dehydration, which increases the adhesion forces between the $TiO_2$-$TiO_2$ particles and $TiO_2$-stainless steel surface (Chen and Dionysiou, 2006b). The final drying temperature of 300 °C showed for both films the highest PL intensity at 300 °C. This indicates that at this final temperature the $TiO_2$ particles showed the optimum adhesion between each other and the stainless steel surface. As the final drying temperature of the film was increased above 300 °C, cracks were formed and $TiO_2$ particles were detached during the washing step, leading to a decrease of $^{\bullet}$OH formation. The formation of cracks is probably due to two reasons: first, the difference of expansion of the stainless steel and the film and second, the increasing contraction of $TiO_2$-$TiO_2$ particles by further dehydration. Nevertheless, choosing the smallest wire diameter possible (0.355 mm) preserved the minimum cracks formation, as by further decreasing of the wire diameter the curvature increases and the possibility of cracks formation increases.

Figure 5b shows the effect of the number of dip coatings on the photocatalytic activity of the coating films. Three dip

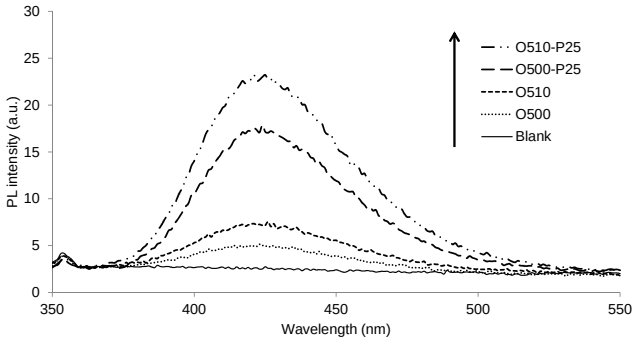


**Figure 4.** PL spectra of 2-OHTA formed by 45 min irradiation of different coated meshes. Initial TA concentration is $5 \times 10^{-4}$ M; excitation is at 315 nm; final drying temperature is 300 °C.

coatings of O500-P25 exhibited the maximum PL intensity at 425 nm when it was irradiated for 45 min with solar light in the presence of a basic TA solution. While the low photocatalytic activity performance for the films coated with O510-P25 sol gel with more than one dip coating was due to its high viscosity which increased the possibility of cracks formation.

Figure 6a shows the microscopic image of the coating films of O500-P25 with different numbers of dip coatings. In the first image the texture of the stainless steel substrate appears clearly as being coated by O500 sol without $TiO_2$-P25. The density of the $TiO_2$ agglomerates is increased by increasing the number of dip coatings of O500-P25. The area covered by the agglomerates per unit surface area of the substrate increased with an increase in the number of dip coatings until three dip coatings. There was no significant increase in the density of $TiO_2$ agglomerates observed by increasing the number of dip coatings from three to five. This explains the increase of the $^{\bullet}OH$ formation from one dip coating to three dip coatings and no further improvement in the photocatalytic activity after three dip coatings.

Figure 6b shows the microscopic image of the coated stainless steel woven mesh with O500-P25 sol gel with three dip coatings at 300 °C. The commercial O500 sol acts as a binder for the $TiO_2$ P-25 Degussa particles agglomerates (Chen and Dionysiou, 2006a). The coating $TiO_2$ film shows a good coverage of the complex woven mesh shape. However, by dipping the mesh in a sol gel and then lifting it, a meniscus surface of the sol was formed and then solidified by heating. As a consequence, this meniscus surface formed film wings. These wings may get detached by attrition causing a damage of the coating film over the mesh wires.

Figure 6c shows the effect of the number of dip coatings with O500-P25 at 300 °C on the average film thickness and roughness. There is a more or less linear relationship between the average film thickness and the number of dip coatings. This is in agreement with what was observed by Chen and Dionysiou (2006c). The average film thickness is approximately 2.2 µm per dip coating. It was found that the photocatalytic activity of a $TiO_2$ thin film reached its maximum at a film thickness of ca. 140 nm (Eufinger et al., 2008) and of 360–430 nm (Nam et al., 2004). The difference between the two studies is due to the difference in the thin film preparation techniques and/or the experimental setup for testing their photocatalytic activity. Tada and Tanaka (1997) proposed that there is a limited diffusion length of the charge carriers and a cumulative light adsorption with increasing film thickness. They found that the critical film thickness is ca. 100–150 nm, from which they deduced a charge carrier diffusion length of about 300 nm. Eufinger et al. (2008) deduced that most of the incoming light is absorbed in the first few 100 nm of the film. Therefore, it can be concluded that the increase in photocatalytic efficiency with an increasing number of dip coatings is not due to the increase in film thickness. Figure 6c shows an increase in average roughness from ca. 1 µm to 2 µm by increasing the number of dip coatings from 1 to 3 Afterwards, no further increase in roughness was observed. This indicates that new $TiO_2$ agglomerates were deposited on the surface of the film by each dip coating until three dip coatings and the active sites on the $TiO_2$ film surface was increased. The conclusion is that the average film roughness is an important parameter for the photocatalytic activity of thick $TiO_2$ films as the critical average film thickness (ca. 6.4 µm) gave the highest average film roughness (ca. 2 µm).

Since adhesion for immobilized $TiO_2$ films is an important property in water treatment, the cross-hatch tape test was performed on the coating films over stainless steel flat plate to evaluate the strength of adhesion. According to ASTM 3359, the result of the adhesion test has been qualitatively divided into 6 grades, from 5 to 0, where grade 5 represents the highest level of adhesion and 0 the lowest level of adhesion. The O500-P25 coating film with three dip coatings at 300 °C showed the best adhesion. About 75 % of the squares of the lattice were not detached after pulling off the tape, corresponding to ASTM Class 2B.

### 3.1.2 Electrophoretic deposition

Figure 7a and b shows the microscopic views of the coated stainless steel woven mesh with O500-P25 sol gel by EPD using DC current (6 V, 2.5 A) during 1 min deposition time. The coating $TiO_2$ film with the EPD method shows better homogeneity than that coating by dip coating method especially with large dimensions. This would be due to the applied electric field which enabled a uniform distribution of $TiO_2$ particles on the mesh surface. Less film wings were observed with EPD method because of the action of the applied electric field which forced the $TiO_2$ particles to attach with mesh wires and prevented the formation of a meniscus between the mesh wires. Figure 7c shows the area covered by the $TiO_2$ agglomerates per unit surface area of the substrate

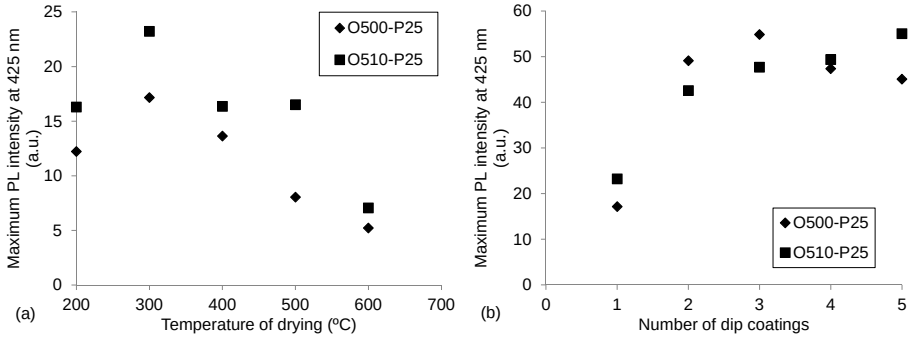


**Figure 5.** Maximum PL intensity at 425 nm for woven meshes coated with O500-P25 and O510-P25 sol solutions as a function of **(a)** final drying temperature (one dip coating) and **(b)** number of dip coatings (final drying at $T = 300\,^{\circ}\mathrm{C}$).

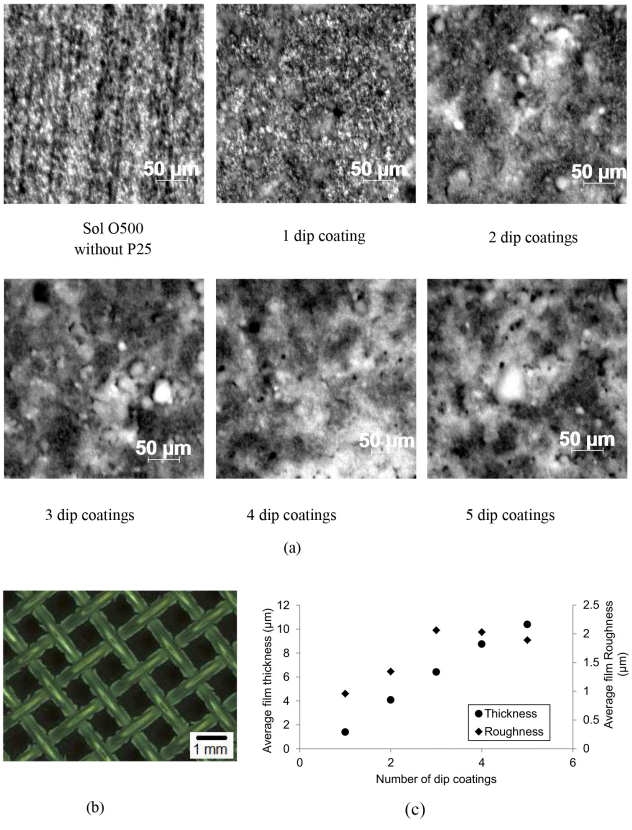


**Figure 6. (a)** Microscopic images of coating films showing increasing of $TiO_2$ agglomerates by increasing of number of dip coatings. **(b)** Microscopic image for woven mesh coated by three dip coatings on O500-P25 sol gel and dried at final temperature 300 °C. **(c)** Average surface thickness and roughness of O500-P25 $TiO_2$ film over stainless steel flat plate with different number of dip coatings at 300 °C measured by Veeco Dektak 8 Stylus Profiler.

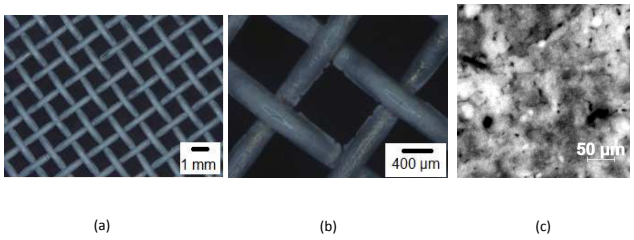


**Figure 7.** Microscopic image of the stainless steel woven mesh coated with EPD method using O-500 sol gel modified with $TiO_2$ suspension: **(a)** low magnification; **(b)** high magnification; **(c)** microscopic image of coating film with O500-P25 sol gel by EPD using DC current (6 V, 2.5 A) during 1 min deposition time.

higher than that obtained with the sol gel dip coating technique.

The $TiO_2$ coating film with EPD shows a little bit better adhesion than that coating by dip coating technique three times using the O500-P25 sol gel. The cross-hatch tape test was performed on the coating film by the EPD technique over stainless steel flat plate. About 80–85 % of the squares of the lattice were not detached after pulling off the tape, corresponding to ASTM Class 2B. On the other hand, EPD technique produced a thicker $TiO_2$ film ranging between 8.95 µm and 9.29 µm with a higher average roughness of 2.2 µm compared to that obtained by dip coating technique three times using the O500-P25 sol gel. This indicates that more $TiO_2$ agglomerates were deposited on the surface of the substrate introducing more active sites for the catalyst and explaining the higher maximum PL intensity obtained by the coating films by EPD technique compared with that obtained by the dip coating technique (see Fig. 7).

Figure 8 shows the formation of 2-OHTA as a PL intensity at 425 nm for the small single woven disc meshes (diameter 5.5 cm) and the large single woven sheet (19 cm × 32 cm) coated by EPD. The area-to-volume ratio for the large mesh was higher than that for the small mesh. Thus, in order to adjust the PL intensity results from the large mesh, they were divided by a factor 2.15. This factor is the result of dividing the area-to-volume ratio of the small mesh ($23.75 \times 10^{-4}\,\mathrm{m^2}\,0.1\,\mathrm{L^{-1}}$) by the area-to-volume ratio of the large mesh ($510 \times 10^{-4}\,\mathrm{m^2}\,1\,\mathrm{L^{-1}}$). The results show a linear relationship between the formation of 2-OHTA and the time.

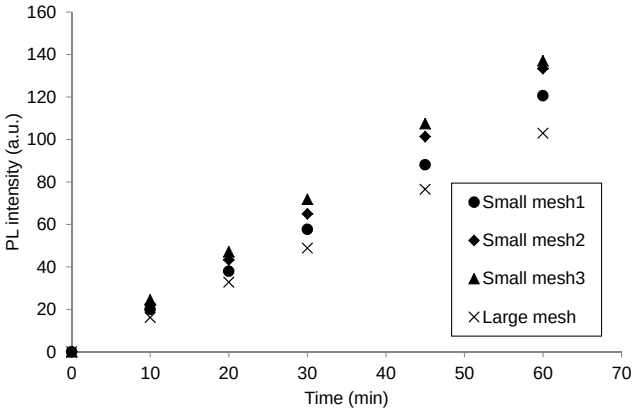


**Figure 8.** Maximum PL intensity at 425 nm as a function of time for three single woven disc meshes and single woven sheet (19 cm × 32 cm), coated by EPD, after corrections for area-to-volume ratio.

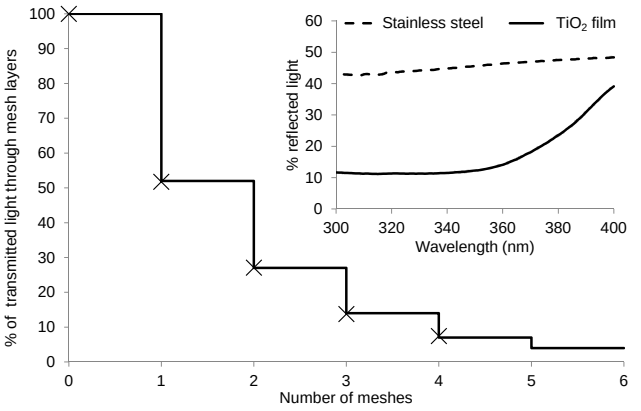


**Figure 9.** Light transmission through uncoated woven meshes (for which $r = 0.48$) in a non-absorbing medium (distilled water). The solid line represents model calculations according to Eq. (1); (×) measured intensities with 1 cm mesh separation. Inset: reflection of stainless steel flat plate and $TiO_2$ film measured with the integrated sphere spectrometer.

The PL intensity results for the large sheet mesh were slightly lower, but of the same order of magnitude, than those for the small disc meshes. This means that the amount of $^{\bullet}OH$ radicals with the large mesh was close to the amount that was produced with the small meshes.

The conclusion was, therefore, that coating of stainless steel woven meshes by the EPD is up-scalable and gives a higher $^{\bullet}OH$ radical production, a lower formation of cracks, and a higher adhesion than the dip coating technique. On the other hand, a comparison between the mesh structure and the flat plate in the fixed-bed reactor on the photodegradation of HA is given in detail by El-Kalliny (2013).

### 3.2 Light distribution in a structure of packed meshes

#### 3.2.1 Light transmission through the mesh structure

Figure 9 shows a comparison between the measured and calculated percentages of the UV light transmitted through uncoated mesh layers immersed in a non-absorbing medium (distilled water). It shows the stepwise decrease of the light intensity at the passage of each mesh according to Eq. (1), while the intensity between the meshes remains constant (solid line). The top ends of the vertical lines represent the light intensity falling on the mesh and the bottom ends represent the light intensity transmitted through the mesh. For a non-absorbing medium, $\varepsilon$ is near to be zero and the right term in Eq. (1) becomes equal to 1. Thus, the reduction of light is due to the mesh layers only, which is represented by the left term in Eq. (1). Using the experimental setup for light distribution measurements described in Sect. 2.3, the light transmission through different stacks of meshes was measured for separation distances of 1 cm. The calculated and the experimental measurements of the intensities of UV solar light in the range of 300–400 nm after passing ($n$) meshes coincide with each other, which validates the model Eq. (1). This indicates that Eq. (1) can be applied to investigate the transmitted light profile not only for meshes immersed in non-absorbing medium but also for those immersed in absorbing medium.

The inset in Fig. 9 shows the reflection of light ($\lambda = 300$–400 nm) for stainless steel and $TiO_2$ film measured by the integrated sphere spectrometer. The largest contribution of reflected light will be experienced by the second mesh: from this mesh the light is reflected upwards and backwards from the down side of the first mesh. The calculation shows that the largest contribution of reflected light is an extra 2 % using stainless steel (average reflection of 40 %) and 0.2 % using $TiO_2$ coated meshes (average reflection of 13 %). This shows that the assumption not to consider back and forth reflection by the meshes in the calculations was justified.

Figure 10 shows the measurements of the percentage of transmitted light through coated woven meshes immersed in a non-absorbing medium (distilled water) at two different separation distances. For coated meshes with an open area of 55 %, $r = 0.45$ due to a slight increase in the mesh wire thickness with coating. The measurement values were more or less the same, indicating that the drop of the light transmission was due to the meshes only and that there was no effect of the separation distances between the mesh layers. In addition, the mesh was like a diffuser which intends to break up the light beams without introducing shadows below it. Thus, the system in practice behaves as an ideal stacked mesh system. Shifting or turning one mesh over the next, there was not an observable influence on the intensity readings, indicating that the transmitted light below the mesh was distributed homogeneously and the homogeneity of the coating film over the mesh was good enough to distribute the light. Practically, the orientation of the meshes was fixed randomly which gave a good opportunity to subject the mesh wires to the light

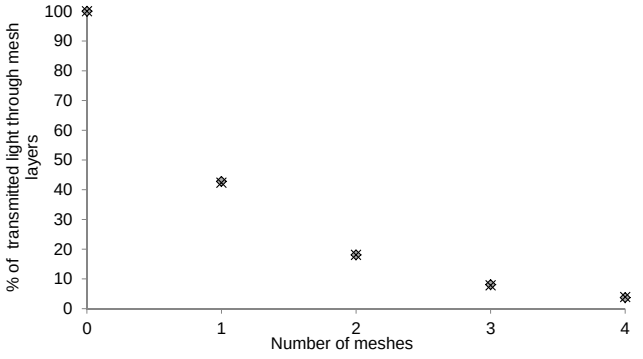


**Figure 10.** Light transmission through coated woven meshes ($r = 0.45$) in a non-absorbing medium (distilled water). Measured intensities: (⧫) 0.2 cm mesh separation; (×) 1 cm mesh separation.

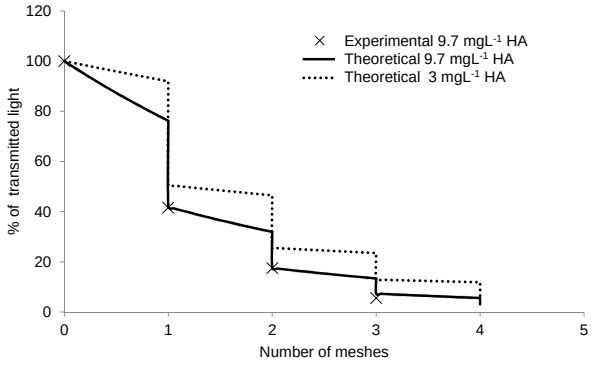


**Figure 11.** Experimental measurements and theoretical calculations for the percentage of the transmitted UV solar light (300–400 nm) through coated woven meshes ($r = 0.45$) with separation distance 1 cm in the presence of different concentrations of HA.

radiation and prevent the shadowing effect. In conclusion, Eq. (1) can be used to calculate the percentage of transmitted light through coated meshes.

### 3.2.2 Effect of a light absorbing medium

The experimental setup for light distribution measurements described in Sect. 2.4 was used for measuring the light transmission through different stacks of meshes for separation distances of 1 cm immersed in a light absorbing medium (9.7 mg $L^{-1}$ HA, which is comparable to the concentration of HA in surface water).

Figure 11 shows a comparison between the measured and calculated percentages of the UV light transmitted through the coated mesh layers and immersed in a light absorbing medium. The curves for the light transmission through the colored water layers follow Lambert Beer's law with an exponential decrease in transmission. Thus the transmitted light through meshes and HA of 3 mg $L^{-1}$ is higher than the one transmitted through meshes and HA of 9.7 mg $L^{-1}$. The measured transmission values of the UV solar light in the wavelength range of 300–400 nm with HA of 9.7 mg $L^{-1}$ coincide with the calculated values. This indicates that Eq. model (1) which describes the transmission of light through mesh layers and Eq. (2) which calculates the fraction of the light absorbed by HA layers can be used to describe the transmission light profile inside the packed bed reactor. The transmission through the coated mesh structure was strongly affected by the presence of a light absorbing medium or colored water due to the absorption of light in the range of 300–400 nm. The lower the transmission values through HA solution, the lower the interaction of light with the catalyst surface was. It was calculated that a maximum of 3.6 % of the incident light irradiated the coated fifth mesh with HA concentration of 3 mg $L^{-1}$. Thus, three, or maximum four meshes, were sufficient to harvest more than 96 % of the irradiated solar light. Figure 11 also shows that as the HA concentration decreased the percentage of the transmitted light through the HA layers increased and consequently the fraction of light available for the production of $^{\bullet}$OH radicals increases. Similarly, as the separation distance between mesh layers decreased the percentage of the transmitted light through the HA layers increased (see Eq. 1). The photocatalytic oxidation efficiency will be the highest when the fraction of the captured light by the meshes available for the production of $^{\bullet}$OH radicals is optimized. This can be done by introducing the dimensionless parameter $\beta = \varepsilon \cdot C \cdot d$ in order to be applicable for various light absorbing mediums with different extinction coefficients and for different concentrations.

The dimensionless parameter $\beta$ approached 0 for very clean water and approximately 1 for highly contaminated water with, for example, HA concentration of 20 mg $L^{-1}$ and a maximum separation distance between the meshes of 2 cm, assuming that there is no shadowing effect that influences the light transmission, where the shadowing effect is not present with a separation distance larger than 0.2 cm (see Fig. 10). This realistic range of $\beta$ is due to that the fine suspended particles were not taken into consideration and the absorbance of light was only due to the dissolved organic materials of HA. Figure 12 shows the decrease in the fraction of the captured light as a function of $\beta$ for systems with different number of meshes. It shows that as $\beta$ increased, less number of meshes is required. Three meshes are enough for capturing the light for $\beta > 0.4$ and two meshes are enough for $\beta > 0.7$ as there is no contribution for the third mesh. This means that with a very low concentration of colored water contaminated with micro-pollutants, a multi mesh system would be used. The intercept of the curves with $y$ axis represent the fraction of the captured light by meshes in the presence of non-absorbing medium.

The separation distance should be low as much as possible in order to decrease the effect of absorption of light with HA layers and decrease the value of $\beta$. The lower separation distance provides a good vertical mixing and a higher captured number of photons per unit reactor volume. Practically, the

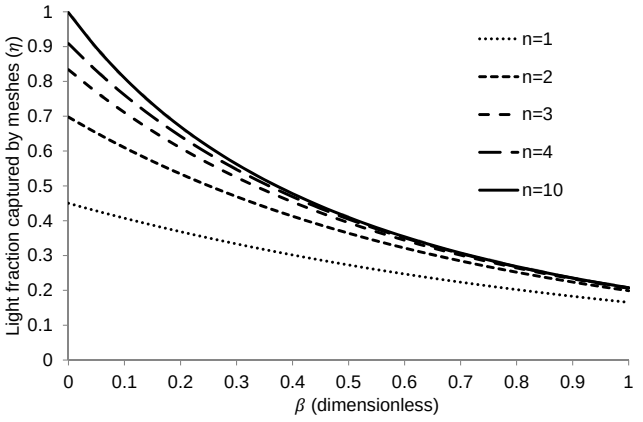


**Figure 12.** The fraction of captured light by the coated meshes ($r = 0.45$) as a function of the dimensionless $\beta$ parameter in a light absorbing medium.

separation distance can be decreased as much as possible to be 0.2 cm in order to avoid any attachment of the mesh layers because the meshes were not flattened perfectly. On one hand, as the open area of the mesh increases, the fraction of light reduced by mesh $r$ decreases and more meshes should be used in order to capture the light as much as possible. On the other hand, as the mesh wire diameter decreases, the surface area increases and the shadowing effect is minimized.

## 4 Conclusions

- The average film roughness is an important parameter for the photocatalytic activity of thick $TiO_2$ films as the critical average film thickness (ca. 6.4 µm) gave the highest average film roughness (ca. 2 µm) in a dip coating technique.
- A promising immobilized photocatalyst was prepared by EPD technique on stainless steel woven meshes using a stable $TiO_2$ suspension in sol gel O500 as electrolyte at 300 °C dryness temperature. This technique shows a higher $^{\bullet}OH$ formation, a lower cracks formation, a better homogeneity and adhesion than dip coating technique. Coating with EPD is up-scalable for large stainless steel woven meshes.
- A stainless steel woven wire mesh was a good photocatalyst substrate due to its large surface area and the possibility of the light to be effectively distributed through it.
- The equation model (1) can be used to describe the distribution of the light through the catalyst woven mesh structure not only immersed in non-absorbing medium, but also in a light absorbing medium.
- The dimensionless parameter $\beta = \varepsilon \cdot C \cdot d$ can be used to optimize the fraction of the captured light by meshes in a colored medium in order to be applicable for various light absorbing mediums with different extinction coefficients and for different concentrations.
- Three mesh layers or maximum four were enough to harvest more than 96 % of the light in the presence of colored water with HA.
- A 0.2 cm separation distance was an optimum separation distance between mesh layers to have as much as possible illuminated light on top of the last mesh layer at the bottom of the reactor. This distance also meets the design criteria of having a high vertical mixing and a high captured number of photons per unit reactor volume.

**Acknowledgements.** This research work has been carried out within the framework of INNOWATOR project, financed by Agentschap NL.

Edited by: A. Verliefde

## References

Balasubramanian, G., Dionysiou, D. D., Suidan, M. T., Baudin, I., and Laîné, J. M.: Evaluating the activities of immobilized $TiO_2$ powder films for the photocatalytic degradation of organic contaminants in water, Appl. Catal. B-Environ., 47, 73–84, 2004a.

Balasubramanian, G., Dionysiou, D. D., and Suidan, M. T.: Titanium dioxide coatings on stainless steel, in: Dekker Encyclopedia of Nanoscience and Nanotechnology, Marcel Dekker, edited by: Schwarz, J. A. and Contescu, C. I., ISBN: 978-0-8247-5055-8, Vol. 6 (Chapter 311), 2004b.

Boccaccini, A. R., Schindler, U., and Krüger, H.-G.: Ceramic coatings on carbon and metallic fibres by electrophoretic deposition, Mater. Lett., 51, 225–230, 2001.

Boccaccini, A. R., Karapappas, P., and Marijuan, J. M.: $TiO_2$ coatings on silicon carbide and carbon fibre substrates by electrophoretic deposition, J. Mater. Sci., 39, 851–859, 2004.

Chen, Y. and Dionysiou, D. D.: $TiO_2$ photocatalytic films on stainless steel: The role of degussa P-25 in modified sol–gel methods, Appl. Catal. B-Environ., 62, 255–264, 2006a.

Chen, Y. and Dionysiou, D. D.: Effect of calcination temperature on the photocatalytic activity and adhesion of $TiO_2$ films prepared by the P-25 powder-modified sol–gel method, J. Mol. Catal. A-Chem., 244, 73–82, 2006b.

Chen, Y. and Dionysiou, D. D. : Correlation of structural properties and film thickness to photocatalytic activity of thick $TiO_2$ films coated on stainless steel, Appl. Catal. B-Environ., 69, 24–33, 2006c.

Chen, Y. and Dionysiou, D. D.: A comparative study on physicochemical properties and photocatalytic behavior of macroporous $TiO_2$-P25 composite films and macroporous $TiO_2$ films coated on stainless steel substrate, Appl. Catal. A-Gen., 317, 129–137, 2007.

Collins-Martínez, V., Ortiz, A. L., and Elguézabal, A. A.: Influence of the anatase/rutile ratio on the $TiO_2$ photocatalytic activity for

the photodegradation of light hydrocarbons, Int. J. Chem. React. Eng., 5, A92, 2007.

Dijkstra, M. F. J., Buwalda, H., de Jong, A. W. F., Michorius, A., Winkelman, J. G. M., and Beenackers, A. A. C. M.: Experimental comparison of three reactor designs for photocatalytic water purification, Chem. Eng. Sci., 56, 547–555, 2001.

El-Kalliny, A. S.: Photocatalytic Oxidation in Drinking Water Treatment Using Hypochlorite and Titanium Dioxide, Ph.D. thesis, Delft University of Technology, Delft, the Netherlands, 85–100, 2013.

Eufinger, K., Poelman, D., Poelman, H., De Gryse, R., and Marin, G. B.: $TiO_2$ thin films for photocatalytic applications in Thin Solid Films: Process and Applications, ISBN: 978-81-7895-314-4, 189–227, 2008.

Feitz, A. J., Boyden, B. H., and Waite, T. D.: Evaluation of two solar pilot scale fixed-bed photocatalytic reactors, Water Res., 34, 3927–3932, 2000.

Fujishima, A., Zhang, X., and Tryk, D. A.: $TiO_2$ photocatalysis and related surface phenomena, Surf. Sci. Rep., 63, 515–582, 2008.

Ghorbani, M.: Electrophoretic deposition of titanium dioxide nanopowders films in isopropanol as a solvent, Int. J. Mod. Phys. B, 22, 2989–2994, 2008.

Goetz, V., Cambon, J. P., Sacco, D., and Plantard, G.: Modeling aqueous heterogeneous photocatalytic degradation of organic pollutants with immobilized $TiO_2$, Chem. Eng. Process., 48, 532–537, 2009.

Goldstein, S., Aschengrau, D., Diamant Y., and Rabani, J.: Photolysis of aqueous $H_2O_2$: quantum yield and applications for polychromatic UV actinometry in photoreactors, Environ. Sci. Technol., 41, 7486–7490, 2007.

Grillon, F., Fayeulle, D., and Jeandin, M.: Quantitative image analysis of electrophoretic coating, J. Mater. Sci. Letters, 11, 272–275, 1992.

Gumy, D., Rincon, A. G., Hajdu, R., and Pulgarin, C.: Solar photocatalysis for detoxification and disinfection of water: Different types of suspended and fixed $TiO_2$ catalysts study, Sol. Energy, 80, 1376–1381, 2006.

Ismail, K. N., Hamid, K. H. K., Kadir, S. A. S. A., Musa, M., and Savory, R. M.: Woven stainless steel wire mesh supported catalyst for $NO_X$ reduction in municipal solid waste flue (MSW) gas: synthesis and characterization, The Malaysian Journal of Analytical Sciences, 11, 246–254, 2007.

Li, F. B., Li, X. Z., Kang, Y. H., and Li, X. J.: An innovative $Ti/TiO_2$ mesh photoelectrode for methyl orange photoelectrocatalytic degradation, J. Environ. Sci. Heal. A, 37, 623-640, 2002.

Li, X. Z., Liu, H. L., and Yue, P. T.: Photoelectrocatalytic oxidation of rose bengal in aqueous solution using a $Ti/TiO_2$ mesh electrode, Environ. Sci. Technol., 34, 4401–4406, 2000.

Li, X. Z., Liu, H. L., Li, F. B., and Mak, C. L. : Photoelectrocatalytic oxidation of rhodamine B in aqueous solution using $Ti/TiO_2$ mesh photoelectrodes, J. Environ. Sci. Heal. A, 37, 55–69, 2002.

Malato, S., Blanco, J., Vidal, A., and Richter, C.: Review: Photocatalysis with solar energy at a pilot-plant scale: An overview, Appl. Catal. B-Environ., 37, 1–15, 2002.

Malato, S., Fernandez-Ibanez, P., Maldonado, M. I., Blanco, J., and Gernjak, W.: Decontamination and disinfection of water by solar photocatalysis: Recent overview and trends, Catal. Today, 147, 1–59, 2009.

McCullagh, C., Skillen, N., Adams, M., and Robertson, P. K. J.: Photocatalytic reactors for environmental remediation: A review, J. Chem. Technol. Biot., 86, 1002–1017, 2011.

Mehrotra, K., Yablonsky, G. S., and Ray, A. K.: Kinetic studies of photocatalytic degradation in a $TiO_2$ slurry system: Distinguishing working regimes and determining rate dependences, Industrial & Engineering Chemical Research, 42, 2273–2281, 2003.

Nam, H.-J., Amemiya, T., Murabayashi, M., and Itoh, K.: Photocatalytic activity of sol-gel $TiO_2$ thin films on various kinds of glass substrates: the effects of $Na^+$ and primary particle size, J. Phys. Chem. B, 108, 8254–8259, 2004.

Parra, S., Stanca, S. E., Guasaquillo, I., and Thampi, K. R.: Photocatalytic degradation of atrazine using suspended and supported $TiO_2$, Appl. Catal. B-Environ., 51, 107–116, 2004.

Pelaez, M., Nolan, N. T., Pillai, S. C., Seery, M. K., Falaras, P., Kontos, A. G., Dunlop, P. S. M., Hamilton, J. W. J., Byrne, J. A., O'Shea, K., Entezari, M. H., and Dionysiou, D. D.: A review on the visible light active titanium dioxide photocatalysts for environmental applications, Appl. Catal. B-Environ., 125, 331–349, 2012.

Sakamoto, R., Nishimori, H., Tatsumisago, M., and Minami, T.: Preparation of titania thick films by electrophoretic sol-gel deposition using hydrothermally treated particles, Journal of Ceramic Society of Japan, 106, 1034–1036, 1998.

Sarkar P. and Nicholson, P. S.: Electrophoretic deposition (EPD): Mechanisms, kinetics, and application to ceramics, J. Am. Ceram. Soc., 79, 1987–2002, 1996.

Shang, J., Li, W., and Zhu, Y.: Structure and photocatalytic characteristics of $TiO_2$ film photocatalyst coated on stainless steel webnet, J. Mol. Catal. A-Chem., 202, 187–195, 2003.

Sunada, K., Watanabe, T., and Hashimoto, K.: Studies on photokilling bacteria on $TiO_2$ thin film, J. Photoch. Photobio. A, 156, 227–233, 2003.

Tada, H. and Tanaka, M.: Dependence of $TiO_2$ photocatalytic activity upon its film thickness, Langmuir, 13, 360–364, 1997.

Thiruvenkatachari, R., Saravanamuth, V., and Moon, I. S.: A review on $UV/TiO_2$ photocatalytic oxidation process, Korean J. Chem. Eng., 25, 64–72, 2008.

Yanagida, S., Nakajima, A., Kameshima, Y., Yoshida, N., Watanabe, T., and Okada, K.: Preparation of a crack-free rough titania coating on stainless steel mesh by electrophoretic deposition, Mater. Res. Bull., 40, 1335–1344, 2005.

Yanagida, S., Nakajima, A., Kameshima, Y., and Okada, K.: Effect of applying voltage on photocatalytic destruction of 1,4-dioxane in aqueous system, Catal. Commun., 7, 1042–1046, 2006.

Yang, H., Zhu, S., and Pan, N.: Studying the mechanisms of titanium dioxide as ultraviolet-blocking additive for films and fabrics by an improved scheme, J. Appl. Polym. Sci., 92, 3201–3210, 2004.

Yigit, Z. and Inan, H.: A study of the photocatalytic oxidation of humic acid on anatase and mixed-phase anatase–rutile $TiO_2$ nanoparticles, Water Air Soil Poll., 9, 237–243, 2009.

Yoon, J., Shim, E., and Joo, H.: Photocatalytic reduction of hexavalent chromium (Cr(VI)) using rotating $TiO_2$ mesh, Korean J. Chem. Eng., 26, 1296–1300, 2009.

Yu, J., Su, Y., and Cheng, B.: Template-free fabrication and enhanced photocatalytic activity of hierarchical macro-/mesoporous titania, Adv. Funct. Mater., 17, 1984–1990, 2007a.

Yu, J., Zhang, L., Cheng, B., and Su, Y.: Hydrothermal preparation and photocatalytic activity of hierarchically sponge-like macro-/mesoporous titania, J. Phys. Chem. C, 111, 10582–10589, 2007b.

Yu, J. and Wang, B.: Effect of calcination temperature on morphology and photoelectrochemical properties of anodized titanium dioxide nanotube arrays, Appl. Catal. B-Environ., 94, 295–302, 2010.

Zhang, W., Li, Y., Wu, Q., and Hu, H.: Removal of endocrine-disrupting compounds, estrogenic activity, and escherichia coliform from secondary effluents in a $TiO_2$-coated photocatalytic reactor, Environ. Eng. Sci., 29, 195–201, 2012.

Ziegmann, M., Doll, T., and Frimmel, F. H.: Matrix effects on the photocatalytical degradation of dichloroacetic acid and atrazine in water, Acta Hydroch. Hydrob., 34, 146–154, 2006.